Supporting Information

One-Dimensional Silicon Nanoshuttles Simultaneously Featuring Fluorescent and Magnetic Property

*Bin Song,‡ Yiling Zhong,‡ Houyu Wang, Yuanyuan Su, and Yao He**

Jiangsu Key Laboratory for Carbon-Based Functional Materials and Devices, Institute of Functional Nano & Soft Materials (FUNSOM) and Collaborative Innovation Center of Suzhou Nano Science and Technology (NANO-CIC), Soochow University, Suzhou 215123, China

E-mail: yaohe@suda.edu.cn

1 Experimental methods

1.1 Materials and devices

The (3-aminopropyl) trimethoxysilane (97%) was purchased from Sigma-Aldrich. Trisodium citrate dihydrate (≥ 99.0%) and ferric chloride (≥ 97.0%) were purchased from Sinopharm Chemical Reagent Co., Ltd (China). CdSe/ZnS QDs were purchased from Wuhan Jiayuan Co., Ltd (China). Rhodamine 6G was purchased from Sigma-Aldrich. All chemicals were used without additional purification. All solutions were prepared using Milli-Q water (Millipore) as the solvent. The microwave system NOVA used for synthesizing materials was made by Preekem of Shanghai, China. The system operated at 2450 MHz frequency and worked at 0-500 W power. Exclusive vitreous vessels with a volume of 15 mL were equipped for the system to provide security during reaction demanding high temperature and pressure. UV-vis absorption spectra were recorded with a Perkin Elmer Lambda 750 UV-vis-near-infrared spectrophotometer. Photoluminescence (PL) measurements were performed using a HORIBA JOBIN YVON FLUOROMAX-4 spectrofluorimeter. The TEM/HRTEM overview images were recorded using Philips CM 200 electron microscope operated at 200 kV. High-resolution X-ray photoelectron spectroscopy (XPS) analyses were performed using a Kratos AXIS Ultra^{DLD} ultrahigh vacuum (UHV) surface analysis system, which consists of a fast entry air lock (base pressure $< 1 \times 10^{-8}$ Torr), a multiport carousel chamber ($< 5 \times 10^{-10}$ Torr), a deposition chamber ($< 5 \times 10^{-10}$ Torr), and an analysis chamber ($< 3 \times 10^{-10}$ Torr). A monochromatic Al Kα source (1486.6 eV) with a resolution of 0.1 eV was used to irradiate the samples. XPS samples were prepared by drop-casting SiNSs (~2 mg) onto aluminum substrates and degassing at 10^{-7} Torr for 15 hours prior to analysis. All XPS spectra were internally calibrated to the C 1s emission (284.8 eV). After calibration, a Shirley-type background was applied to remove most of the extrinsic loss structure. Secondly, to minimize sample charging, the charge neutralizer filament was used when required. FTIR measurements, KBr was pressed into a slice, onto which the SiNSs sample was dropped. The solvent in the sample was adequately evaporated by irradiation (> 30 min) with a high-power incandescent lamp. FTIR spectra were recorded on a Bruker HYPERION FTIR spectrometer and cumulated 32 scans at a resolution of 4 cm^{-1}. The powder X-ray diffraction (XRD) spectra were recorded on a PANalytical, Empyrean, X-ray diffractometer with Cu Kα radiation,

operated at 40 mA and 40 kV. The materials were placed dropped on zero-background sample holder made of monocrystal silicon plate. Energy-dispersive X-ray (EDX) spectroscopy was utilized to determine the fraction of the resultant materials. TEM and HRTEM samples were prepared by dispersing the sample onto carbon-coated copper grids with the excess solvent evaporated. The TEM/HRTEM overview images were recorded using Philips CM 200 electron microscope operated at 200 kV. A Raman microscope (HR800) equipped with a 633 nm He-Ne 20 mW laser (polarized 500:1) was employed for obtaining the Raman spectra. The acquisition and analysis of Raman data were performed by using the LabSpec5 software. The probe beam was a 370 nm laser beam (with a repetition frequency of 1 MHz). TGA analysis was performed on a METTLER TOLEDO TGA/STDA 851 instrument. The samples, which ranged in weight from 5 to 12 mg, were placed in a porcelain crucible and heated under air atmosphere from 30 to 700 °C at a rate of 10 °C/min. Measurements of magnetic properties were performed using a Quantum Design MPMS magnetometer based on a superconducting quantum interference device (SQUID; Quantum Design, Inc.) and vibrating sample magnetometer (VSM; VSM Model EV9, MicroSense, LLC). Our samples were scanned under a 3 T clinical MRI scanner (Bruker Biospin Corporation, Billerica, MA, USA) at room temperature. After acquiring the T_1-and T_2-weighted MR images, the intensities of images were measured within manually drawn regions of interest for each sample. Relaxation rates were calculated from T_1 and T_2 values at different iron concentrations.

1.2 Synthesis of SiNSs

The precursor solution was prepared by adding 2 ml of (3-aminopropyl) trimethoxysilane to 8 ml N_2-satureted aqueous solution dispersed with 0.075 g of trisodium citrate. Then, 0.05 mmol iron (III) chloride was mixed into the citric acid aqueous solution under constant stirring. The mixture was stirred for 30 min. The resultant precursor solution was transferred into the exclusive vitreous vessel with a volume of 15 ml. The SiNSs were prepared under 150 ^{o}C/30 min. To exclude impurities influence, such as (3-aminopropyl) trimethoxysilane molecules, trisodium citrate and iron (III) chloride in solution, the residual reagents were removed by dialysis (500 Da). The samples of SiNSs were separated through centrifugation at 5000 rpm for 10 min to achieve the pure SiNSs free of impurity. In addition, our method is effica-cious for synthesis of high-quantity SiNSs, e.g., 0.032 g SiNSs are

readily achieved in a 30 min reaction. The purified SiNSs are then used for following characterizations and applications.

1.3 Photostability stability of SiNSs

The photoluminescence intensity of R6G, CdSe/ZnS QDs, carbon dots, SiNPs and SiNSs were adjusted to the same value. The three samples were continuously irradiated for different time intervals using a xenon lamp of 365 nm.

1.4 Photoluminescent quantum yields (PLQY) measurements

PLQY, well considered as an important factor for quantitatively evaluating fluorescent intensity of materials, equals to the ratio of the number of emitted photons and the number of absorbed photons. In our experiment, a well-established reference method was employed for determining the PLQY value of SiNSs as follow (Quinine sulfate in 0.1 M H_2SO_4 (literature quantum yield: 58%)).[1]

$$\Phi_x=\Phi_{st}\,(I_x/I_{st})\,(\eta_x/\eta_{st})^2\,(A_{st}/A_x)$$

Where Φ is the QY, "I" is the integrated emission intensity, "η" is the refractive index of the solvent, and A is the optical density. The subscript "st" and "x" stand for standard with known QY and the SiNSs sample, respectively. To minimize reabsorption effects, absorption value at the excitation wavelength is required to be smaller than 0.10.

1.5 Nanocrystal size calculation

The XRD patterns index to diamond cubic Si. The peak broadening can be used to calculate the nanocrystal size by using the Scherrer equation:

$$D = K\lambda/B\cos\theta$$

In equation, D is the nanocrystal diameter, K is a constant related to morphology, B is the full width at half-maximum (fwhm) in radians, and θ is the scattering angle.

1.6 Microwave synthesis of SiNPs and carbon nanodots

Fluorescent silicon nanoparticles (SiNPs) were readily achieved through microwave synthesis based on previous reports.[2a] In details, The SiNPs precursor solution was

prepared by adding 1 mL (3-aminopropyl) trimethoxysilane to 8 mL N_2-saturated aqueous solution dispersed with 0.075 g trisodium citrate dihydrate. The mixture was stirred for 10 min. The resultant precursor solution was transferred into the exclusive vitreous vessel with a volume of 30 mL. The SiNPs were prepared under 150 °C/60 min. To exclude impurities influence, the residual reagents were removed by dialysis (500 Da). The purified SiNPs aqueous solution was used for characterizations. The blue-emitting carbon nanodots (C-dots) were synthesized through our previously reported microwave synthesis.[2b] In brief, 20 mL milk was first put into the vessel and heated to 175 °C for 25 min. When cooled down to room temperature, the obtained solid was dialyzed using pure water through a dialysis membrane (500 Da). The purified C-dots were finally collected for photostability comparison.

2. Additional data

Figure S1 shows TEM, HRTEM images and UV-PL spectra of the prepared SiNPs.

Figure S2 shows the PLQY and reaction yield of SiNSs as a function of reaction temperature.

Figure S3 shows the PLQY and reaction yield of SiNSs as a function of Fe^{3+} concentrations.

Figure S4 shows the length distribution analysis and DLS spectra of prepared SiNSs.

Figure S5 shows the FTIR spectrum the prepared SiNSs.

Figure S6 shows the EDX spectrum the prepared SiNSs.

Figure S7 shows the Raman spectrum of the prepared SiNSs.

Figure S8 shows the XPS spectra of the SiNSs.

Figure S9 shows the TGA profiles of the prepared SiNSs.

Figure S10 shows the PL decay curves of the prepared SiNSs.

Figure S11 shows the temperature-dependent magnetization moments of the prepared SiNSs in zero-field-cooled and field-cooled processes.

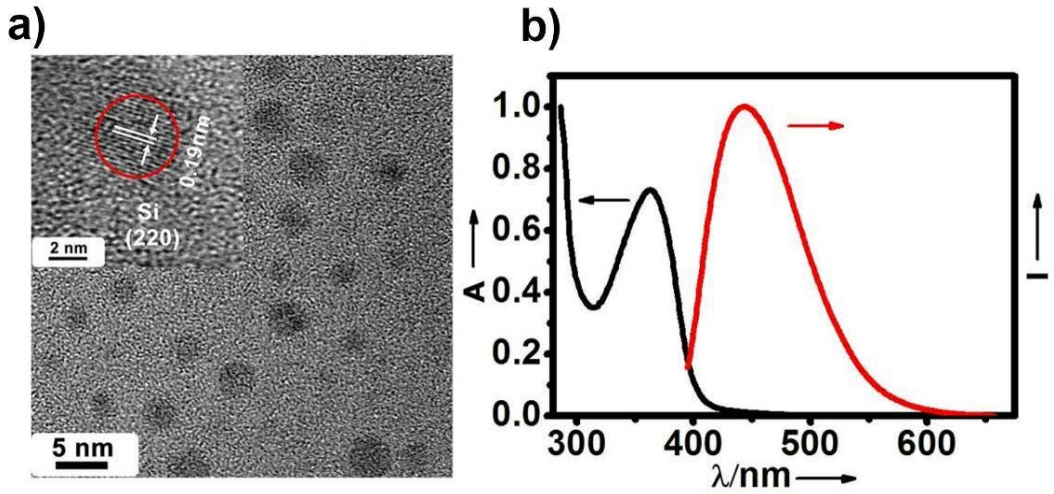

Figure S1. (a) TEM and HRTEM images (inset) and (b) UV-PL spectra of the as-prepared SiNPs. The SiNPs show spherical structures with sizes of ~2-3 nm, and exhibit clearly resolved absorption peak and symmetrical PL peak.

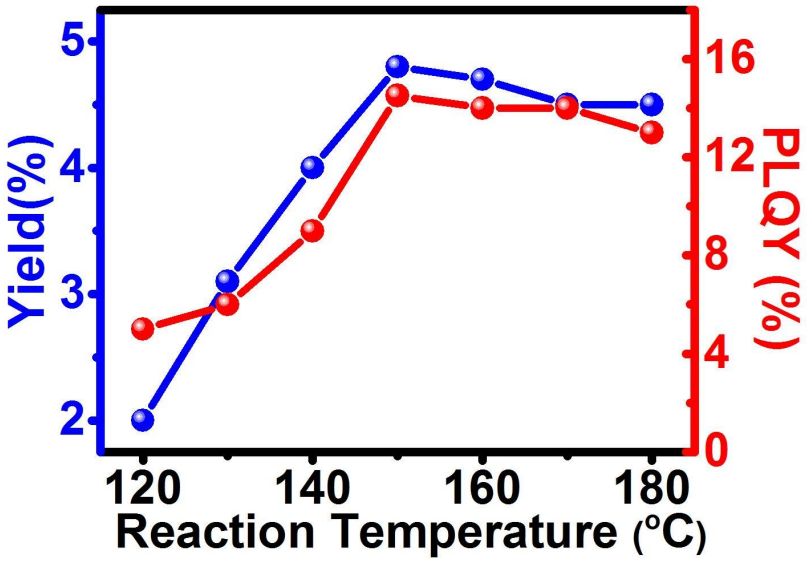

Figure S2. The SiNSs PLQY (red line) and SiNSs reaction yield (blue line) as a function of reaction temperature. Obviously, at initial stage, the PLQY value is enhanced with the increase of reaction temperature; and the highest PLQY of 15% is obtained between 150 °C and 160 °C. Accordingly, the reaction yield increases from 2.1% to 4.7% as the temperature increases to 150 °C, indicating a temperature-dependent crystallization process. The high PLQY and reaction yield is achieved at high reaction temperature due to the high nucleation rate. Therefore, we choose 150 °C as reasonable reaction temperature in the following experiment.

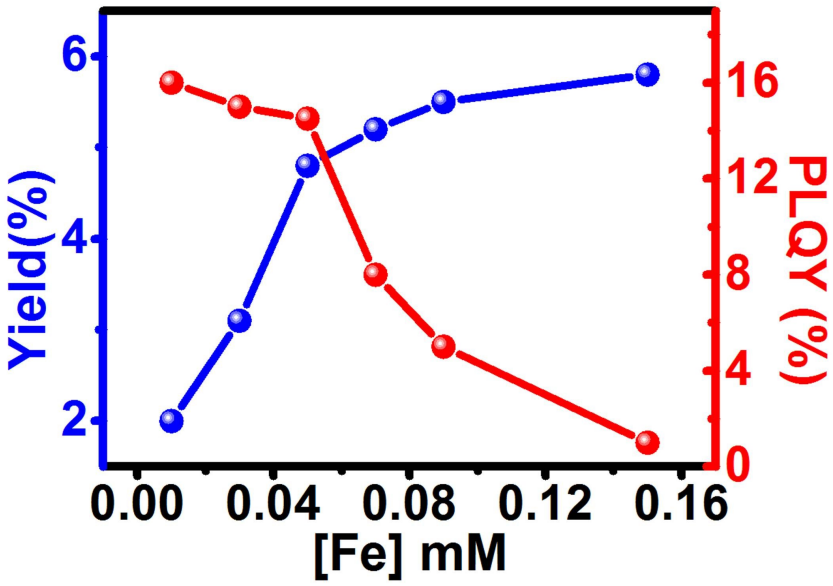

Figure S3. The SiNSs PLQY (red line) and SiNSs reaction yield (blue line) as a function of Fe^{3+} concentrations (reaction temperature: 150 ^{o}C). The highest quantum yield of 16% is observed for the sample with Fe^{3+} concentration of 0.01 mM, while the sample with Fe^{3+} concentration of 0.05 mM has a quantum yield of 15%. When the Fe content increases to 0.15 mM, the quantum yield decreases to 1%. Because the Fe^{3+} may bring about the generation of Fe-related impurity levels localized within the optical band gap of shuttle. The Fe-related impurity levels act as non-radiative recombination sites which lead to the decrease in the PLQY.[3] Accordingly, the reaction yield increases from 2.0% to 5.6% as the Fe^{3+} concentration increases from 0.01 mM to 0.15 mM.

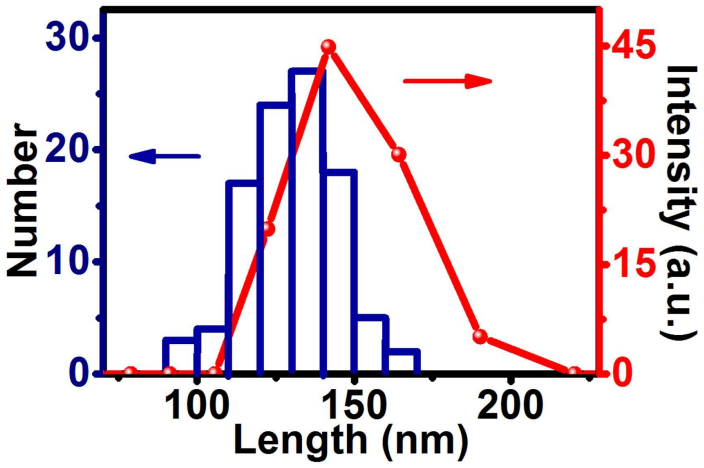

Figure S4. The length distribution analysis (histograms) determined by TEM and DLS spectra (red curves) of as-prepared SiNSs. The length distribution of SiNSs in Figure S4, calculated by measuring more than 100 SiNSs in the TEM image, shows an average length of 135 ± 4 nm, similar to that (~150 nm) confirmed by dynamic light scattering (DLS).

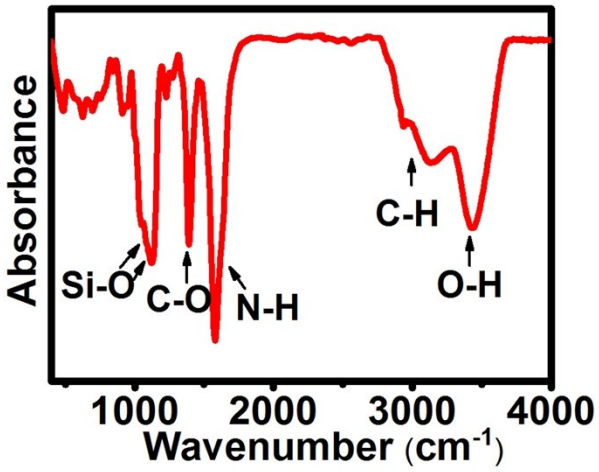

Figure S5. For the Fourier transform infrared spectroscopy (FTIR), the 3200-3700 cm^{-1} region is corresponding to the -OH and -NH stretching vibration. A sharp absorbance peaks at 1000-1200 cm^{-1} are attributed to the Si-O-Si asymmetric stretch vibrations. The 400-800 cm^{-1} region is ascribed to O-Si-O bending vibrations. The strong absorbance at 1390-1440 and 1580 cm^{-1} are, respectively, assigned to the C-O and N-H bending vibrations. The FTIR results demonstrate that the resultant SiNSs have a large amount of amino groups and carbon-related matrix.[4]

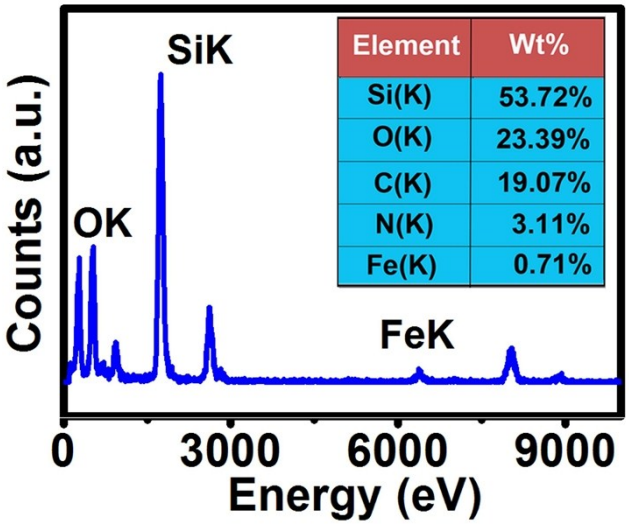

Figure S6. The Energy-dispersive X-ray (EDX) pattern reveals that the SiNSs contain Si, O, C, N and Fe of 53.72, 23.39, 19.07, 3.11 and 0.71 wt% concentration, respectively. It is worthwhile to point out that, for EDX measurement, a quantitative analysis of the elemental ratios is not possible since the supporting substrate (e.g., carbon-coated copper girds) was carbon containing a measurable amount of residual oxygen.

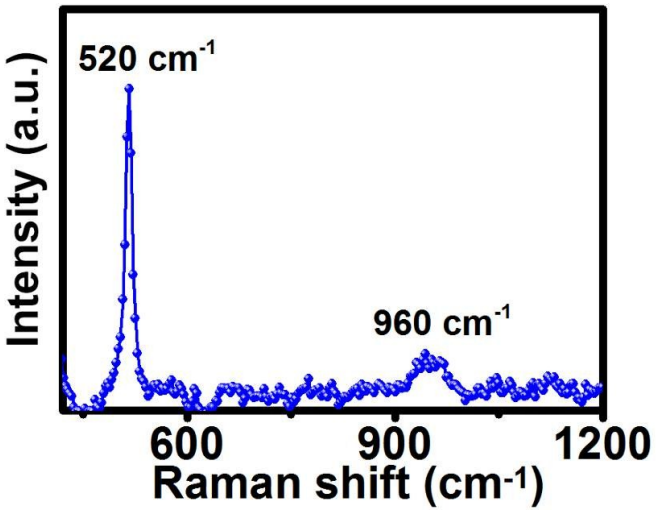

Figure S7. A Raman spectrum is employed for characterization of the prepared SiNSs, showing two significant Raman peaks around 520 cm^{-1} and 960 cm^{-1} produced by crystalline silicon.[5]

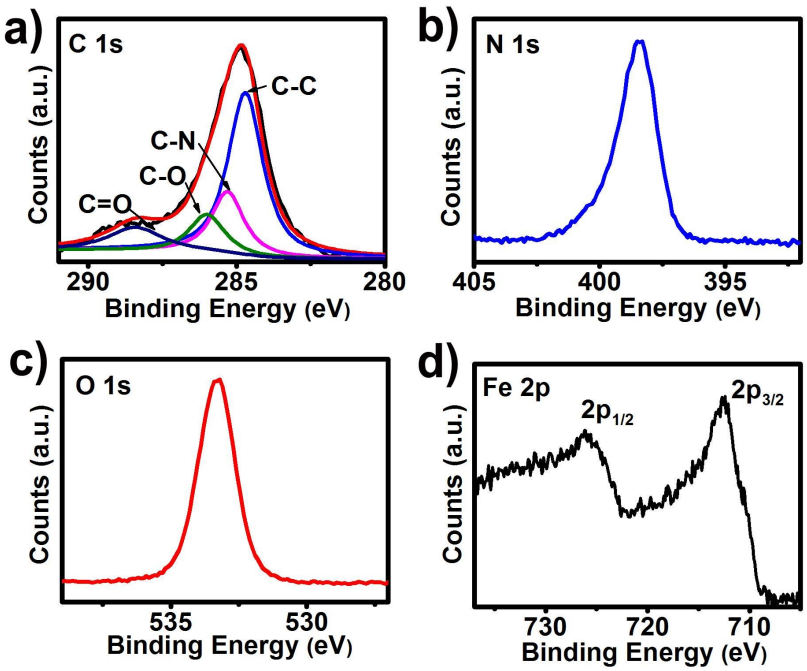

Figure S8. (a) C 1s, (b) N 1s, (c) O 1s and (d) Fe 2p XPS spectra of the prepared SiNSs. As shown in (a) presents the typical C 1s spectrum, exhibiting four distinct peaks located at 284.8, 285.3, 286.1, and 288.5 eV, which are ascribed to C-C, C-N, C-O, and C=O, respectively. In particular, the peaks at 398 eV and 533 eV (ascribed to N 1s and O 1s) are observed in the high-resolution XPS spectrum (b and c), demonstrating the existence of N and O elements in the SiNSs. For the Fe 2p spectrum, two peaks at 726.4 and 712.2 eV are observed, which are ascribed to the $2p_{1/2}$ and $2p_{3/2}$ (d), respectively.[6]

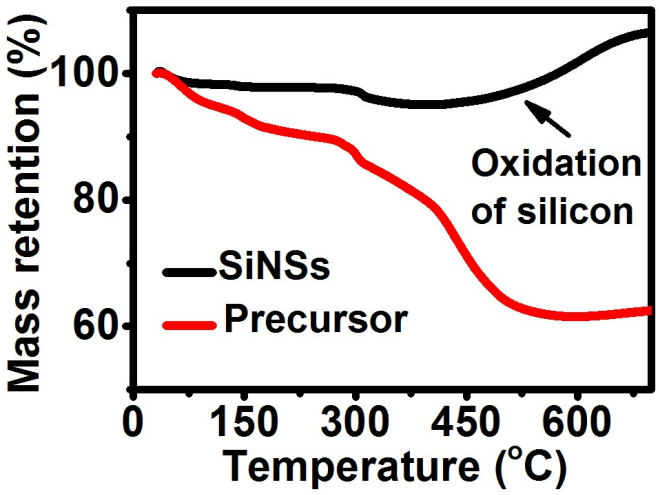

Figure S9. TGA profiles of SiNSs (black line) and precursor (red line). To further study the weight loss/gain of the sample at high temperature, we carry out thermogravimetric analysis. As shown in Figure S6, rapid mass loss between 150 and 480 °C is observed for the precursor (red line), which is ascribed to the burning of carbonous residues. Comparatively, the as-prepared SiNSs remain stable in this temperature range (i.e., 150-480 ^{o}C), while exhibit a noticeable weight increase above 600 ^{o}C resulted from Si oxidation ($Si + O_2 \rightarrow SiO_2$). This data implies the SiNSs samples contain scanty carbon compared to the precursor, and further confirms the high purity of the formed silicon materials.[7]

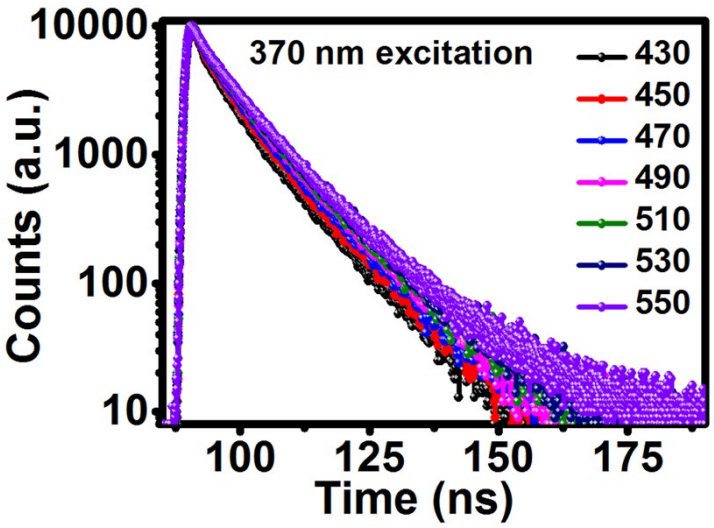

Figure S10. Time-resolved fluorescence-decay curves of SiNSs ($\lambda_{exitation}$=370 nm).

Typically, the fluorescence lifetime spectra of SiNSs (i.e., ~6.95 ns) are consistent with other time-scale (ns) of defect-related emission from silicon nanomaterials with strong blue fluorescence, suggesting the strong blue fluorescence of SiNSs is also from the exciton recombination at localized defect states, occurred at the surfaces of silicon nanomaterials. Here, multiwavelength analyses indicate that the fluorescence decay is rather heterogeneous throughout the measured range. In particular, the luminescence tends to be longer lived in the blue region, that is, around 430 nm, than in the red, around 550 nm with average lifetimes of 5.15 and 6.95 ns, respectively. Furthermore, these measurements afford luminescence time profiles that are best fit by triexponential fitting functions. This suggests several kinds of emission centers within the SiNSs, providing valuable information for fluorophore efficiency improvement.[8]

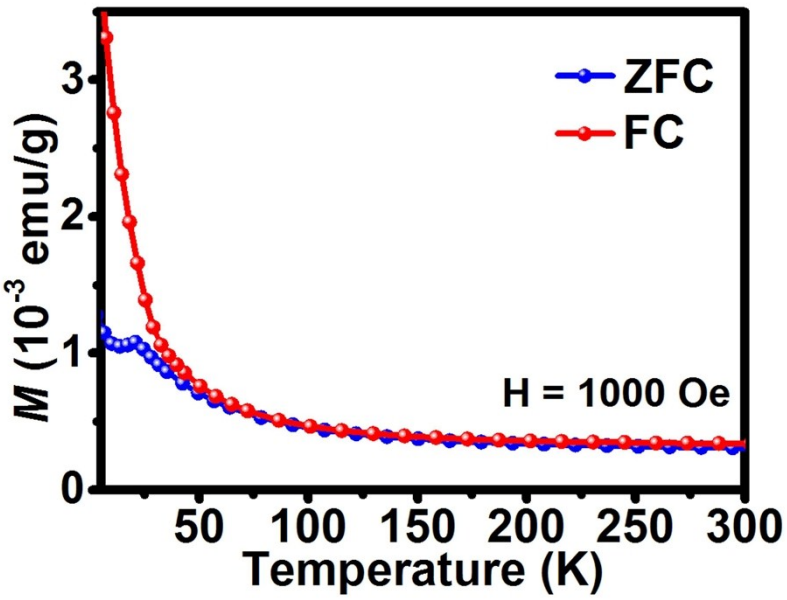

Figure S11. The zero-field-cooled (ZFC) and field-cooled (FC) magnetization curves under a magnetic field of 1000 Oe. The ZFC curve is obtained by cooling the sample in the absence of a magnetic field from 300 to 5 K, and subsequently measuring the magnetic moments while the sample is warmed under a field of 1000 Oe. For the FC process, the sample is cooled through its Curie temperature in the presence of a magnetic field. As shown in Figure S11, the temperature-dependent ZFC and FC curves have a magnetic transition at ~49 K, indicating that the Curie temperature of the SiNSs is ~49 K. Such low Curie temperature suggesting Fe (III) ions as the origin of paramagnetic and ferromagnetic properties of the SiNSs.[9]

References

(1) H. Qin, Y. Niu, R. Meng, X. Lin, R. Lai, W. Fang, X. Peng, *J. Am. Chem. Soc.,* 2014, **136**, 179-187.

(2) (a) Y. L. Zhong, F. Peng, F. Bao, S. Y. Wang, X. Y. Ji, L. Yang, Y. Y. Su, S. T. Lee, Y. He, *J. Am. Chem. Soc.,* 2013, **135**, 8350-8356; (b) J. Wang, F. Peng,; Y. M. Lu, Y. L. Zhong, S. Y. Wang, M. F. Xu, X. Y. Ji, Y. Y. Su, L. S. Liao, Y. He, *Adv. Optical Mater.,* 2015, **3**, 103-111.

(3) K. Sato, S. Yokosuka, Y. Takigami, K. Hirakuri, K. Fujioka, Y. Manome, H. Sukegawa, H. Iwai, N. Fukata, *J. Am. Chem. Soc.,* 2011, **133**, 18626-18633.

(4) M. A. Islam, T. K. Purkait, M. H. Mobarok, I. M. D. Hoehlein, R. Sinelnikov, M. Iqbal, D. Azulay, I. Balberg, O. Millo, B. Rieger, J. G. C. Veinot, *Angew. Chem. Int. Ed.,* 2016, **55**, 7393-7397.

(6) G. Zatryb, P. R. J. Wilson, J. Wojcik, J. Misiewicz, P. Mascher, A. Podhorodecki, *Phys. Rev. B,* 2015, **91**, 235444-235455.

(7) (a) S. N. Qu, X. Y. Wang, Q. P. Lu, X. Y. Liu, L. J. Wang, *Angew. Chem. Int. Ed.,* 2012, **51**, 12215-12218; (b) C. M. Kane, A. Banisafar, T. P. Dougherty, L. J. Barbour, K. T. Holman, *J. Am. Chem. Soc.,* 2016, **138**, 4377-4392; (c) J. Z. Wang, C. Zhong, S. L. Chou, H. K. Liu, *Electrochem Commun*., 2010, **12**, 1467-1470.

(8) K. Sato, S. Yokosuka, Y. Takigami, K. Hirakuri, K. Fujioka, Y. Manome, H. Sukegawa, H. Iwai, N. Fukata, *J. Am. Chem. Soc.,* 2011, **133**, 18626-18633.

(9) (a) S. Ohkoshi, S. Ikeda, T. Hozumi, T. Kashiwagi, K. Hashimoto, *J. Am. Chem. Soc.,* 2006, **128**, 5320-5321; (b) L. Cheng, Z. Chen, S. Ma, Z. Zhang, Y. Wang, H. Xu, L. Yang, G. Han, K. Jack, G. Lu, J. Zou, *J. Am. Chem. Soc.,* 2012, **134**, 18920-18923.